Theor. Appl. Climatol. 71, 231–249 (2002)

Theoretical and Applied Climatology

[1] Group of Micrometeorology, Department of Atmospheric Sciences, Institute of Astronomy and Geophysics, University of São Paulo, São Paulo, SP, Brazil
[2] Laboratory of Solar Radiation, Department of Environmental Sciences, State University of São Paulo – UNESP, Botucatu, SP, Brazil

Diurnal evolution of solar radiation at the surface in the city of São Paulo: seasonal variation and modeling

A. P. de Oliveira[1], **A. J. Machado**[1], **J. F. Escobedo**[2], and **J. Soares**[1]

With 14 Figures

Received September 7, 2000
Revised June 5, 2001

Summary

Seasonal variations in the diurnal evolution of the global, diffuse and direct solar radiation at the surface, the clearness index, diffuse fraction and direct fraction are described in detail for the City of São Paulo, Brazil. The description is based on measurements of global and diffuse solar radiation carried out over 5.25 years. The diffuse component was measured with a shadow-band device. The annual evolution of the amplitude of the diurnal cycle of all radiometric parameters indicates a seasonal pattern with two distinct periods: autumn-winter and spring-summer. About 10% of the observed period was characterized by clear sky days. This seasonal variation is determined by a larger incidence of clear sky days in the autumn-winter period. Reductions of up to 10% in hourly and daily values of global radiation were observed in conjunction with an increase in particulate matter concentration on clear sky days. The pollution effect may be responsible for the discrepancy, of 16%, found between local and more regional estimates of global solar radiation in São Paulo. The diurnal evolution of hourly values of monthly-averaged global and diffuse solar radiation were successfully estimated by the empirical expressions derived here. Daily values of monthly-averaged global solar radiation were satisfactorily estimated using the Angstrom expression.

1. Introduction

Knowledge of the seasonal evolution of global, diffuse and direct solar radiation, at the surface, is important for climate studies, solar collector efficiency estimation, and agricultural and several meteorological applications (Iziomon and Aro, 1999; Iqbal, 1983; Duffie and Beckman, 1980). Unfortunately, these quantities are not available, at the required spatial and temporal resolution, for Brazil. With most of its territorial area (8.547 million km^2) located in equatorial and tropical latitudes, Brazil has a very sparse solarimetric network. For instance, Pereira et al. (1996) reported only 22 ground stations with global solar radiation measured directly or estimated from sunshine hours. In addition, there is no available information in the literature about the diurnal evolution of global, diffuse and direct solar radiation, at the surface, and their seasonal variation for any location in Brazil. The importance and difficulties of estimating the hourly distribution of solar radiation have been emphasized by Aguiar and Collares-Pereira (1992).

The major reason for the lack of direct measurements of diffuse and direct components of the solar radiation, at the surface in Brazil, is that these parameters require special instruments such as sun-tracking pyrheliometers or occulted pyranometers with shadow-bands or disks. These apparatus are expensive, difficult to operate on a regular basis and require the use of correction factors in order to compensate for the distortion

effects caused by the blocking device (Le Baron et al., 1990).

Due to the operational problems described above, most of measurements available in Brazil are carried out in urban areas. This is not only peculiar to Brazil, it happens in other parts of the world (Longuetto et al., 1992). Direct measurements of global, diffuse and direct solar radiations based on pyranometers, pyrheliometers and other similar sensors are likely to be affected by the urban environment. For instance, air pollution may either modify the performance of sensors or alter the radiative properties of the urban atmosphere. Therefore, any application that requires extrapolation of local solar radiation measurements beyond urban limits will also have to take into consideration the role played by urban effects (Petterson et al., 1978; Oke, 1982).

To investigate the inherent difficulties associated with the operation of solar radiation measurements in a regular basis and to identify the effects caused by the urban environment on the spatial representativeness of these measurements, an experimental site was set up in the City of São Paulo (Oliveira et al., 1996). At this site, measurements of global and diffuse solar radiations have been taken regularly since April 1994. These measurements follow WMO recommendations (WMO, 1971) and have been carried out by using a fully automatic data acquisition system. The diffuse component of solar radiation, at the surface, has been measured by a shadow-band device (Mello, 1993; Escobedo et al., 1997).

The City of São Paulo, with 10 million habitants, together with 38 other smaller cities, form the Metropolitan Region of São Paulo (MRSP). This region is occupied by 16.5 million habitants distributed over an area of 8051 km^2 and it is the largest urban area in South America and one of the 10 largest in the world. Therefore, it is an ideal place to investigate the role played by the urban environment on solar radiation.

The MRSP, with more than 4 million motor vehicles (CETESB, 1999), is characterized as having moderate degree of contamination by particulate matter and other pollutants (Kretzschmar, 1994). Oliveira et al. (1996) detected a reduction of up to 18% in the direct beam associated with a progressive increase in the concentration of particulate matter during a period of five cloudless days in the City of São Paulo. According to the authors, depletion of the direct beam was partially compensated by an increase in diffuse solar radiation at the surface. The long-term effects caused by particulate matter on the solar radiation field in São Paulo are still not known.

To characterize the seasonal variation of hourly values of global, diffuse and direct components of solar radiation, at the surface of São Paulo City, a solar radiation dataset with 5.25 years of measurements is used.

The seasonal variations in the diurnal evolution of global, diffuse and direct solar radiations, at the surface, are presented in detail in this work because no similar scientific information, about São Paulo City, is available in the literature. It is hoped that this information will improve understanding of the behavior of the solar radiation field in other urban subtropical areas.

A description of the seasonal variation of the clearness index, diffuse and direct fractions is also included here, once these quantities have been intensively applied to develope correlation models to estimate diffuse solar radiation at the surface (Liu and Jordan, 1960; Collares-Pereira and Rabl, 1979; Erbs et al., 1982; LeBaron and Dirmhirn, 1983; Soler, 1990; Satyamurty and Lahiri, 1992; Garrison and Sahami, 1995; Jacovides et al., 1996).

Special effort has been applied to quantify the impact caused by: (a) the aging effect of the pyranometers (8-years old) on all measurements of solar radiation; (b) the blocking effect caused by the shadow-band device applied to measure diffuse solar radiation and (c) the effects of particulate matter on the global and diffuse solar radiation. These effects are particularly important for understanding solar radiation measurements carried out in other urban environments where air pollution may affect the performance of the sensors and modify properties measured systematically by them.

Another motivation for this work concerns energy production and its associated environmental impact. The energy consumption in the MRSP is around 40 TWh per year (Eletropaulo, 1999). This is a significant fraction of all energy produced in Brazil and it is generated basically by hydroelectric power plants. To increase production of energy, Brazil is looking for other sources of energy because the available hydroelectric

power sources have been practically used up. Moreover, considering the environmental impact associated with the others available sources – nuclear, coal and gas burning power plants – solar radiation has to be prioritized by the local policymaker. The solar radiation information, contained in this work, can also provide a reference for better management of solar energy in the region.

2. Site, instrumentation and data set

The global and diffuse components of solar radiation, at the surface, have been regularly measured in the City of São Paulo, Brazil, since April of 1994. The diffuse component has been measured directly using a shadow-band device. These measurements were taken on a platform located at the top of the building of the IAGUSP (''Instituto Astronômico e Geofisico da Universidade de São Paulo'') at the ''Cidade Universitária Campus'', in the west side of the City of São Paulo, at 744 m amsl (23°33′35″S, 46°43′55″W). Hereafter this measurement site will be called *IAG site* (Fig. 1).

The City of São Paulo is located in the State of São Paulo, Brazil, at approximately 770-m amsl and 60-km west of the Atlantic Ocean (Fig. 1). Its climate – typical of subtropical regions of Brazil – is characterized by a dry winter during June–August and a wet summer during December–March (Fig. 2). The minimum values of daily monthly-averaged temperature and relative humidity occur in July and August (16 °C and 74%,

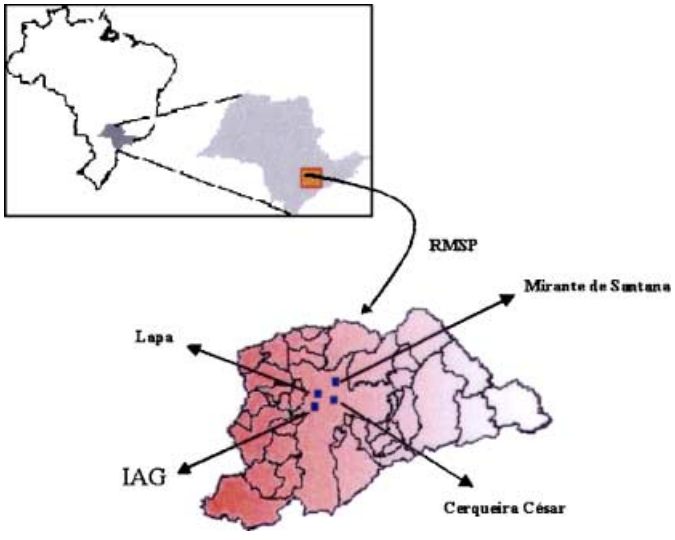

Fig. 1. Geographic position of RMSP, Região Metropolitana de São Paulo (top). The boundaries of São Paulo City and the position of observational sites: IAG, Mirante de Santana, Lapa e Cerqueira Cesar (bottom)

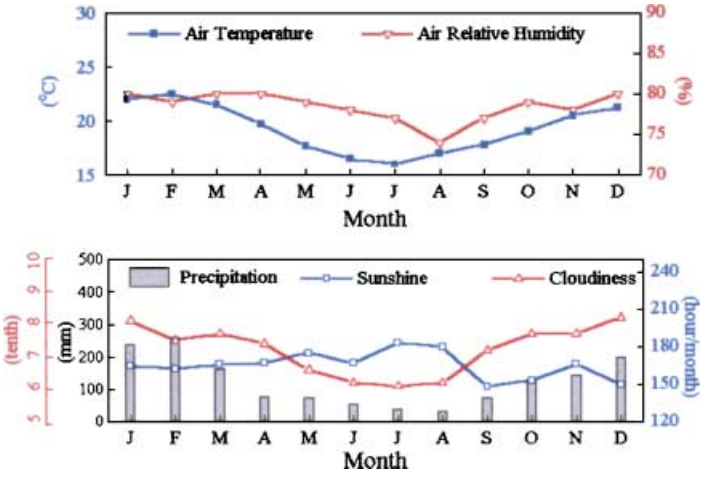

Fig. 2. Seasonal variation of air temperature and relative humidity (top) and precipitation, sunshine hours and cloudiness (bottom). Air temperature, relative humidity and cloudiness correspond to monthly-averaged values. Precipitation and sunshine hours correspond to monthly-accumulated values. These observations were carried out during 1960–1990 at Mirante de Santana. (Data provided by INEMET)

respectively), and the minimum monthly-accumulated precipitation occurs in August (35 mm). The maximum value of daily monthly-averaged temperature occurs in February (22.5 °C) and the maximum value of daily monthly-averaged relative humidity occurs from December through January and from March through April (80%). The maximum value of monthly-accumulated precipitation occurs in February (255 mm). The shortest and the longest day light duration is 10.6 hours (June) and 13.4 hours (December) when the sun reaches the maximum elevation of 54° and 89°, respectively. The maximum value of monthly accumulated sunshine periods occurs in July (183 hours) and the minimum in September (149 hours). The maximum daily monthly-averaged cloudiness occurs in December (8.2 tenths) and the minimum in July (6.1 tenths).

The information displayed in Fig. 2 was based on observations carried out during 1960–1990 in an area called ''Mirante de Santana'' in the northern portion of São Paulo City, approximately 10 km away from the IAG site (Fig. 1). The data was provided by INMET (INEMET, 2000).

Values of global and diffuse solar radiation, used in this work, were measured at the surface, from April 26, 1994 to June 30, 1999, with a sampling frequency of 0.2 Hz (Oliveira et al., 1996). After careful data inspection, 1352 days were selected – with global and diffuse radiation measured simultaneously – to characterize the seasonal variation of solar radiation over the region. This time period corresponds to 71.5% of the whole period of observations (1892 days) and covers 60 of the total 63 months (Fig. 12).

Global solar irradiance and its diffuse component were measured by a pyranometer model 8–48 (SN28455) and model 2 (SN28513F3) respectively; both built by Eppley Lab. Inc. These sensors were calibrated periodically using as secondary standard another spectral precision pyranometer model 2 – (Eppley) (SN28120F3).

In the period considered here 37 calibration constants were estimated. For both pyranometers, the averaged value of these 37 calibration constants were assumed to be the actual value of the calibration constant. For the pyranometer used to measure diffuse solar radiation (model 2), the actual value for calibration constant was $8.17 \pm 0.12\,\mu Vm^2/W$. This is about 4.4% smaller than its nominal value (provided by the manufacturer). In the case of pyranometer used to measure global solar radiation (model 8–48), the actual value was $8.93 \pm 0.13\,\mu Vm^2/W$, which is about 3.5% greater than its nominal value. These variations are within the intervals obtained, for a 95% confidence level, for the averaged values of solar radiation; therefore they can be neglected from the statistical point of view. The fractions resulting from the combination of these estimates (using actual calibration constant) varied from 3.5% to 7.9% also within the interval of the statistical error for a 95% confidence level.

The diffuse component of the solar radiation was measured using a shadow-band device developed by the Laboratory Solar Radiation of UNESP (Mello, 1993; Escobedo et al., 1997). The shadow over the pyranometer, in this device, is produced by a circular band with 40.5 cm of radius and 10.0 cm of width, oriented in such way that its axis is always parallel to Earth's axis. The position of the circular band does not change in time; the seasonal variation of the shadow's position is compensated, displacing the occulted pyranometer horizontally.

Compared to other devices commercially available, this new device has a lower cost and is much easier to operate (Mello, 1993). Details about the impact caused by the ring on the measurements of solar radiation has been fully addressed in the literature for this particular device. The effect produced by shadow-ring over the diffuse solar radiation has been investigated by Panitzer (1981), Ineichen et al. (1984), Steven (1984), Stanhill (1985), Rawlins and Readings (1986), Siren (1987) and LeBaron et al. (1990). In general, the correction factor (F_c) is estimated from the expression: $F_c = (1 - X/T)^{-1}$, where X/T corresponds to the ratio between the fraction of diffuse radiation intercepted by the shadow-band and the total diffuse radiation incoming on the horizontal surface.

The blocking effect produced by the shadow-band used in São Paulo was taken into consideration for all measurements of diffuse solar radiation reported here considering:

$$\frac{X}{T} = \left(\frac{2b}{\pi R}\right)\cos(\delta)\left[\frac{\cos(\phi+\delta)}{\cos(\phi)}\right]^2\left[\int_0^{\omega_p}\cos(z)d\omega\right] \quad (1)$$

where $\int_0^{\omega_p} \cos(z)d\omega$ corresponds to the integral of cosine of solar zenith angle with respect to its hourly angle ω, over the angle corresponding to a half-day period ω_p. Expression (1) was derived considering the geometrical properties of the shadow band and assuming an isotropic diffuse radiation field (Burek et al., 1988; Le Baron et al., 1990).

The correction factor, in the case of São Paulo, reaches a maximum value of 1.235 in summer, when the distance between the shadow-band and the pyranometer is the smallest (37.125 cm). Close to the winter solstice, the F_c drops to 1.052, when the distance between the shadow-band and the pyranometer is the largest (54.271 cm).

To verify the performance of the correction factor, a set of values of diffuse solar radiation measured by the shadow band and estimated by a pyrheliometer were compared. Figure 3 illustrates the results (a) without correction and (b) using the correction factor.

The pyrheliometer used here is a model NIP, manufactured by Eppley (SN28247E6) and it was set up near the shadow band (~ 3 meters). The direct solar radiation component was estimated using a calibration constant provided by the manufacturer ($9.09 \pm 0.05\,\mu Vm^2/W$). In this case, the diffuse solar radiation – assumed as the value of reference – was estimated as the difference between the global and the direct radiations.

As can be seen in Fig. 3, the regression line gets significantly closer to the diagonal line when the correction factor is applied.

Despite the apparent improvement, compensated values of diffuse solar radiation were, on average, 10% smaller than those estimated by the pyrheliometer. This discrepancy can be attributed to the fact that expression (1) does not take into consideration anisotropy of the diffuse solar radiation field. The value of this discrepancy is comparable to the correction proposed by the literature (Steven, 1984). Given the fact that there was little guidance on applying corrections for anisotropy effects, the values of diffuse radiation used in this work were only compensated by geometric effects incorporated in expression (1).

All solar radiation quantities used in this work are expressed as units of megajoules per unit of area (MJ/m^2) and correspond to the flux of energy in any of the three intervals of time: one hour or one day or one month. The flux of energy (E) associated with the global solar radiation at the surface are indicated by E_G^h, E_G^d and E_G^m, where subscript G refers to the global solar radiation and the superscripts h, d and m refer to time intervals of one hour, one day and one month, respectively. Equivalent symbols are used for the diffuse (E_{DF}^h, E_{DF}^d, E_{DF}^m) and the direct (E_{DR}^h, E_{DR}^d, E_{DR}^m) components of the global solar radiation at the surface. In this work the direct solar radiation at the surface was always estimated as the difference between the global and its diffuse component observed at the surface. The flux of energy received from the sun at the top of the atmosphere, per unit of area, and per interval of time of 1 hour or 1 day or 1 month (E_T^h, E_T^d, E_T^m) is estimated analytically (Iqbal, 1983) considering the solar constant equal to $1366\,W/m^2$ (Fröhlich and Lean, 1998). Hereafter, the energy fluxes of solar radiation per unit of area, per interval of time of 1 hour or 1 day or

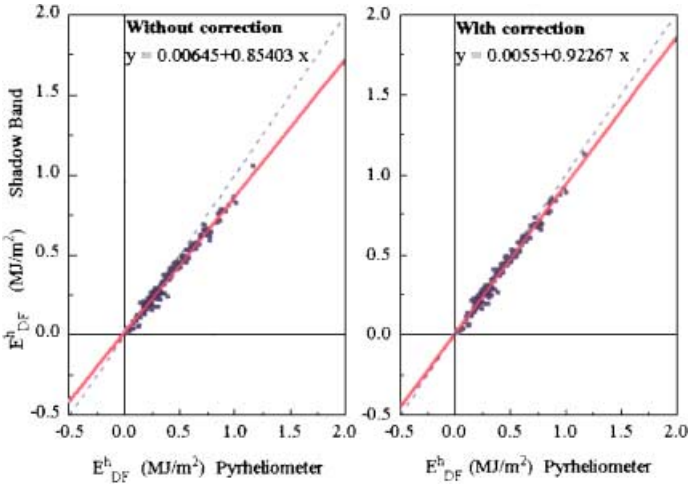

Fig. 3. Hourly values of diffuse solar radiation measured by shadow band versus pyrheliometer, at IAG, during 17 days in 1997 (May 9–13, July 8–16 and August 18–19). Dashed lines correspond to diagonal and continuous lines correspond to curve fitted by least squares method. The correspondent linear equations are indicated in the top of each diagram

1 month will be referred to as *hourly*, *daily and monthly values* and their monthly – averaged values are indicated by "⟨ ⟩".

Seasonal variation of solar radiation fractions, described in this work, are based on monthly averaged hourly, daily and monthly values of solar radiation quantities. The clearness index is expressed as $\langle K_T^h \rangle = \langle E_G^h \rangle / \langle E_T^h \rangle$ and $\langle K_T^d \rangle = \langle E_G^d \rangle / \langle E_T^d \rangle$; diffuse fraction as: $\langle K_{DF}^h \rangle = \langle E_{DF}^h \rangle / \langle E_G^h \rangle$ and $\langle K_{DF}^d \rangle = \langle E_{DF}^d \rangle / \langle E_G^d \rangle$; direct fraction as $\langle K_{DR}^h \rangle = \langle E_{DR}^h \rangle / \langle E_G^h \rangle$ and $\langle K_{DR}^d \rangle = \langle E_{DR}^d \rangle / \langle E_G^d \rangle$. Fractions involving monthly values are not indicated above because they are identical to the ones involving daily values. Fractions with E_T in the denominator are not significantly affected by the order in which the average is

Table 1. Monthly and annual-averaged values and respective errors of the parameters displayed in the figures indicated in parenthesis. Hourly values correspond to 12:30 LT. For clear sky condition the parameters and respective errors were obtained by adjusting a Gaussian curve to their respective distribution

	June (Winter)			December (Summer)		
Parameter	Hourly (MJ/m^2)	Daily (MJ/m^2)	Monthly (MJ/m^2)	Hourly (MJ/m^2)	Daily (MJ/m^2)	Monthly (MJ/m^2)
$\langle E_T \rangle$	3.221 ± 0.002 (Figure 7)	22.12 ± 0.02 (Figure 8)	665 ± 00 (Figure 9)	5.000 ± 0.001 (Figure 7)	42.50 ± 0.01 (Figure 8)	1317 ± 00 (Figure 9)
$\langle E_G \rangle$	1.800 ± 0.057 (Figure 7)	11.17 ± 0.34 (Figure 8)	334 ± 06 (Figure 9)	2.474 ± 0.084 (Figure 7)	19.28 ± 0.54 (Figure 8)	593 ± 24 (Figure 9)
$\langle E_{DF} \rangle$	0.519 ± 0.023 (Figure 7)	3.76 ± 0.12 (Figure 8)	113 ± 05 (Figure 9)	1.212 ± 0.036 (Figure 7)	9.83 ± 0.21 (Figure 8)	306 ± 08 (Figure 9)
$\langle E_{DR} \rangle$	1.281 ± 0.070 (Figure 7)	7.41 ± 0.39 (Figure 8)	221 ± 08 (Figure 9)	1.262 ± 0.091 (Figure 7)	9.46 ± 0.62 (Figure 8)	287 ± 29 (Figure 9)

	June (Winter)		December (Summer)	
Parameter	Hourly (%)	Daily and Monthly (%)	Hourly (%)	Daily and Monthly (%)
$\langle K_T \rangle$	55.9 ± 1.8 (Figure 10)	50.5 ± 1.5 (Figure 10)	49.4 ± 1.9 (Figure 10)	45.4 ± 1.3 (Figure 10)
$\langle K_{DF} \rangle$	28.8 ± 1.6 (Figure 11)	33.6 ± 2.5 (Figure 11)	47.4 ± 2.2 (Figure 11)	51.0 ± 1.8 (Figure 11)
$\langle K_{DR} \rangle$	71.2 ± 4.0 (Figure 6)	66.4 ± 5.0 (Figure 11)	52.6 ± 2.4 (Figure 6)	49.0 ± 1.7 (Figure 11)
$\langle E_{DF} \rangle / \langle E_T \rangle$	16.1 ± 0.7 (Figure 10)	17.0 ± 0.5 (Figure 10)	24.2 ± 0.7 (Figure 10)	23.1 ± 0.5 (Figure 10)
$\langle E_{DR} \rangle / \langle E_T \rangle$	39.8 ± 2.2 (Figure 5)	33.5 ± 1.8 (Figure 10)	25.2 ± 1.8 (Figure 5)	22.3 ± 1.5 (Figure 10)

Annual Average			Clear Sky	
Parameter	Hourly (%)	Daily (%)	Parameter	Daily (%)
$\langle K_T \rangle$	51.5 ± 2.2 (–)	45.9 ± 1.1 (Figure 10)	K_T^d	65.4 ± 1.1 (Figure 13)
$\langle K_{DF} \rangle$	41.8 ± 2.3 (–)	45.7 ± 2.2 (Figure 11)	K_{DF}^d	21.3 ± 1.6 (Figure 13)
$\langle K_{DR} \rangle$	58.2 ± 3.2 (–)	54.3 ± 2.6 (Figure 11)	K_{DR}^d	78.7 ± 5.9 (Figure 13)
$\langle E_{DF} \rangle / \langle E_T \rangle$	21.3 ± 0.9 (–)	20.8 ± 0.7 (Figure 10)	E_{DF}^d / E_T^d	13.7 ± 0.8 (Figure 13)
$\langle E_{DR} \rangle / \langle E_T \rangle$	30.2 ± 2.2 (–)	25.1 ± 1.6 (Figure 10)	E_{DR}^d / E_T^d	51.7 ± 1.8 (Figure 13)

applied because, during the interval of one month, E_T does not vary much for the City of São Paulo (Table 1). Therefore, it can be assumed that $\langle E_G\rangle/\langle E_T\rangle \approx \langle E_G/E_T\rangle$, $\langle E_{DF}\rangle/\langle E_T\rangle \approx \langle E_{DF}/E_T\rangle$ and $\langle E_{DR}\rangle/\langle E_T\rangle \approx \langle E_{DR}/E_T\rangle$ with a high degree of accuracy. On the other hand, fractions with E_G in the denominator are strongly affected by the order in which the monthly-average is applied; in general, the ratio $\langle E_{DF}\rangle/\langle E_G\rangle$ is smaller than $\langle E_{DF}/E_G\rangle$. Observations in São Paulo indicate that $\langle E^h_{DF}\rangle/\langle E^h_G\rangle = -0.112 + 0.984\langle E^h_{DF}/E^h_G\rangle$ and $\langle E^d_{DF}\rangle/\langle E^d_G\rangle = -0.076 + 0.982\langle E^d_{DF}/E^d_G\rangle$, with a linear correlation coefficient near one in both cases.

3. Seasonal variability of the diurnal evolution of the radiation components

June and December will be considered in this work as representative, respectively, of winter and summer for the region of the City of São Paulo because they contain the shortest (10.6 hours) and the longest (13.4 hours) days of the year. They also occupy the center of the autumn–winter and spring–summer periods, April–August and September–March, respectively.

The diurnal evolution of $\langle E^h_G\rangle$, $\langle E^h_{DF}\rangle$, $\langle E^h_{DR}\rangle$, $\langle E^h_T\rangle$ in June and December are indicated in Fig. 4. According to this figure: (a) all quantities present a very well defined diurnal cycle, with a maximum between 12:00 and 13:00 LT (vertical dashed lines in Fig. 4) and (b) the size of the error bars (for a level of 95% of confidence) are small compared to the amplitude of the diurnal cycle.

Feature (a) is observed in all months of the year and therefore the amplitude of the diurnal cycle of the solar radiation components can be specified by the observed value between 12:00 and 13:00 LT in the City of São Paulo. Feature

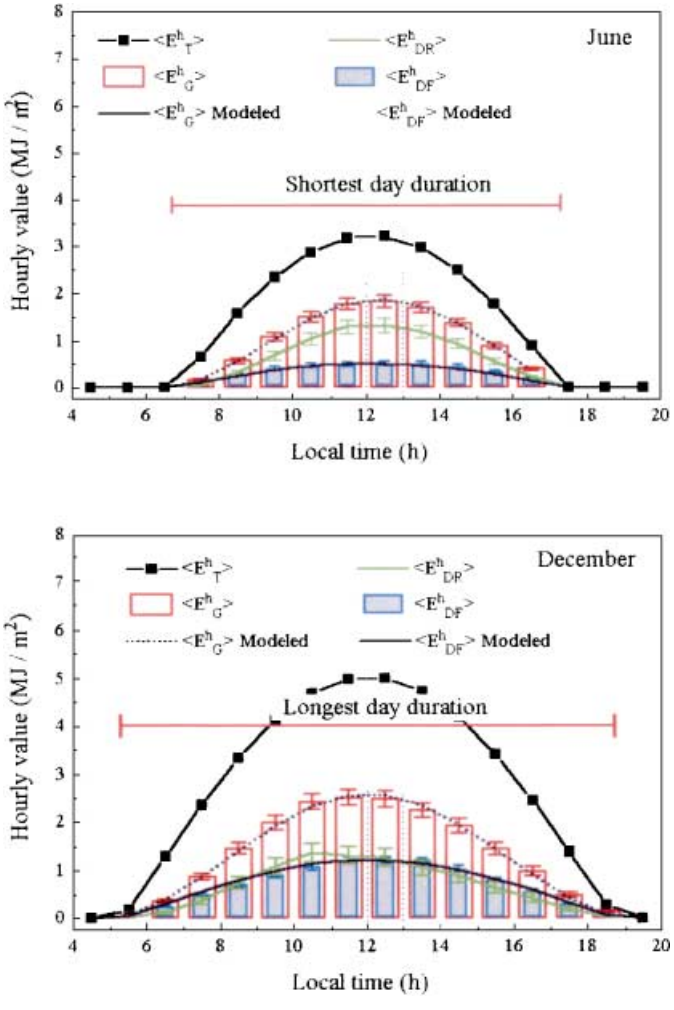

Fig. 4. Diurnal variation of observed $\langle E^h_T\rangle$, observed $\langle E^h_{DR}\rangle$, observed and modeled $\langle E^h_G\rangle$ and observed and modeled $\langle E^h_{DF}\rangle$ in June (top) and December (bottom), at IAG. The error bars correspond to 95% confidence interval. Horizontal line corresponds to the duration of the day. The dotted vertical lines indicate the 12 LT and 13 LT

(b) indicates that the 5.25-year data set, used here, is representative of the mean conditions in the City of São Paulo.

The daytime evolution of $\langle K_T^h \rangle$, $\langle E_{DF}^h \rangle / \langle E_T^h \rangle$ and $\langle E_{DR}^h \rangle / \langle E_T^h \rangle$ (Fig. 5) and the daytime evolution of $\langle K_{DF}^h \rangle$ and $\langle K_{DR}^h \rangle$ (Fig. 6) show a very well defined diurnal cycle, with the size of the error bars (at the 95% confidence level) small in comparison to their amplitudes. The amplitude of the diurnal cycle can also be represented by their values between 12:00 LT. and 13:00 LT. (vertical dashed lines in Figs. 5 and 6).

The parameters $\langle K_{DF}^h \rangle$ and $\langle K_{DR}^h \rangle$ have statistical errors larger than $\langle K_T^h \rangle$ because they contain the combined effect of the statistical errors existent in $\langle E_G^h \rangle$ and $\langle E_{DF}^h \rangle$, and in $\langle E_G^h \rangle$ and $\langle E_{DR}^h \rangle$, respectively. The parameters $\langle E_{DF}^h \rangle / \langle E_T^h \rangle$ and $\langle E_{DR}^h \rangle / \langle E_T^h \rangle$ present a distribution of statistical errors similar to $\langle K_T^h \rangle$.

In general, the time evolution of $\langle K_T^h \rangle$, $\langle K_{DR}^h \rangle$ and $\langle E_{DR}^h \rangle / \langle E_T^h \rangle$ indicate the presence of a maximum between 12:00 and 13:00 LT, and a minimum at sunrise and sunset. On the other hand, $\langle E_{DF}^h \rangle / \langle E_T^h \rangle$ remains constant during the daytime period, and $\langle K_{DF}^h \rangle$ shows a minimum between 12:00 and 13:00 LT and two maximums, one at sunrise and the other at sunset. These patterns were observed in all months of the year. The symmetry around noontime is less pronounced in the summer months due to the increase of cloud activity during the afternoon (Figs. 5 and 6, bottom).

The anomalous large values of $\langle K_T^h \rangle$ and $\langle E_{DF}^h \rangle / \langle E_T^h \rangle$ observed in the end of the day, during

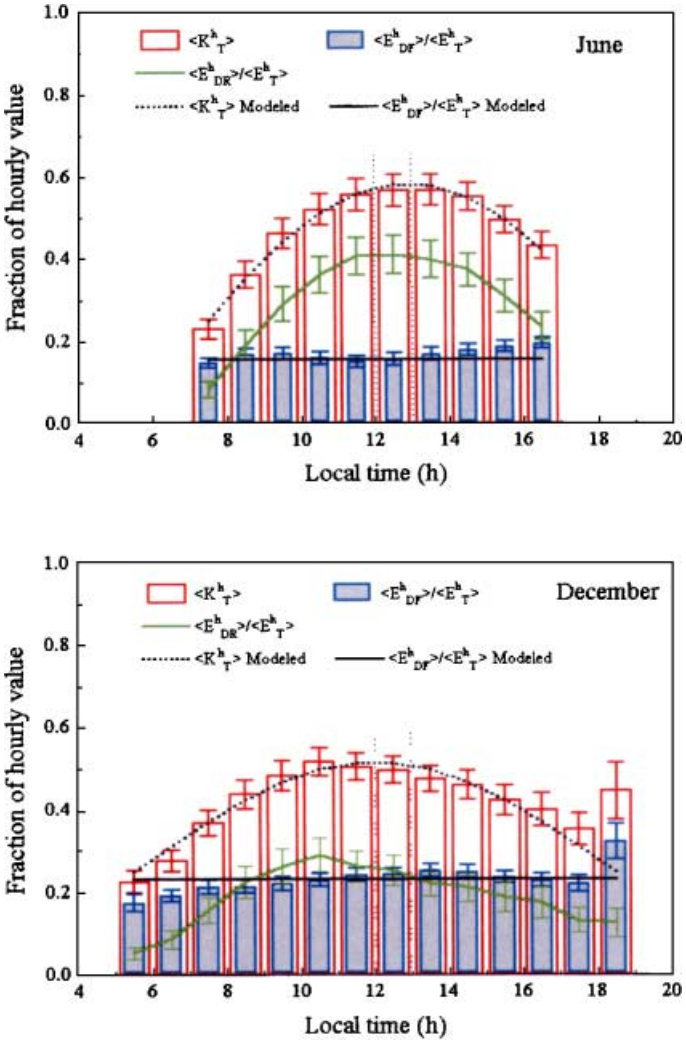

Fig. 5. Diurnal variation of observed and modeled $\langle K_T^h \rangle$, observed and modeled $\langle E_{DF}^h \rangle / \langle E_T^h \rangle$ and observed $\langle E_{DR}^h \rangle / \langle E_T^h \rangle$ in June (top) and December (bottom) at IAG. The error bars correspond to 95% confidence interval. The dotted vertical lines indicate the 12 LT and 13 LT

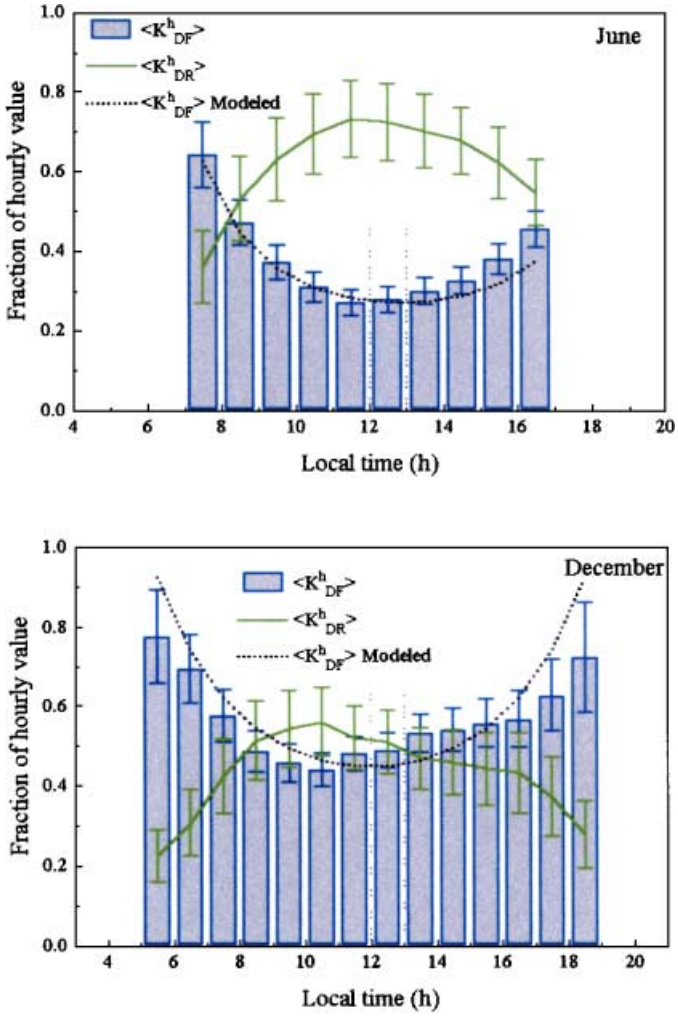

Fig. 6. Diurnal variation of observed $\langle K^h_{DR} \rangle$ and observed and modeled $\langle K^h_{DF} \rangle$ during June (top) and December (bottom), at IAG. The error bars correspond to 95% confidence interval. The dotted vertical lines indicate the 12 LT and 13 LT

the summer period (Fig. 5, bottom) may be related to horizon and cloud reflection effects.

4. Seasonal variability of hourly, daily and monthly radiation components

To characterize the seasonal variability of the solar radiation in the City of São Paulo the annual evolution of the clearness index and radiation fractions are displayed in Figs. 7 to 11.

The amplitude of the diurnal evolution of energy fluxes is given by the values at 12:00 and 13:00 LT and indicated by 12:30 LT in Fig. 7. The annual evolution of energy flux daily values is shown in Fig. 8 and of energy flux monthly values in Fig. 9. The annual evolution of $\langle K^d_T \rangle$, $\langle K^d_{DF} \rangle$, $\langle K^d_{DR} \rangle$ and other related fractions are displayed in Figs. 10 and 11. For reference, their respective numerical values for June and December are indicated in Table 1.

An important characteristic found in the annual evolution of all these parameters is that the error bars are small, for a 95% confidence, level compared to the amplitude of theirs annual cycle.

4.1 Seasonal variability of energy fluxes

The annual evolution of the amplitude of monthly-averaged hourly, daily and monthly values (Figs. 7, 8 and 9) is strongly correlated with the annual evolution of cloudiness and sunshine hours in the region of São Paulo (Fig. 2). During autumn–winter periods, the monthly-averaged precipitation and cloudiness are smaller than in the spring–summer period (Fig. 2, bottom). The annual evolution of the monthly-averaged sunshine hours presents a reverse behavior.

In terms of diurnal evolution, it is observed that in June the amplitude of $\langle E^h_G \rangle$ and $\langle E^h_{DF} \rangle$ is,

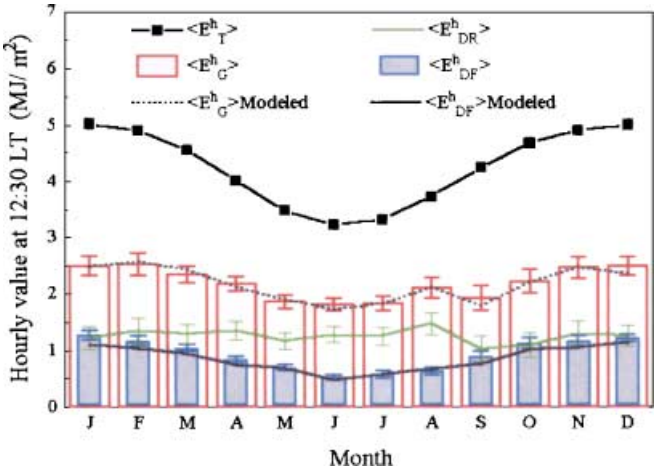

Fig. 7. Annual variation of hourly values of solar radiation components, based on monthly-averaged hourly values observed at 12:30 LT at IAG. The modeled values of flux of energy associated to global and diffuse solar radiations are also displayed. The error bars correspond to 95% confidence interval

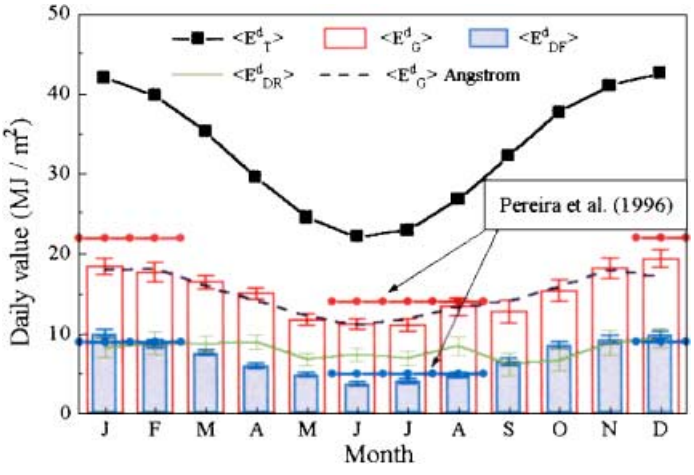

Fig. 8. Annual variation of daily values of solar radiation observed at IAG. The error bars correspond to 95% confidence interval. The horizontal solid-circle lines correspond to daily values of global and diffuse solar radiation for the region of São Paulo provided by Pereira et al. (1996). The black dashed line represents the global solar radiation estimated using Angstrom formula

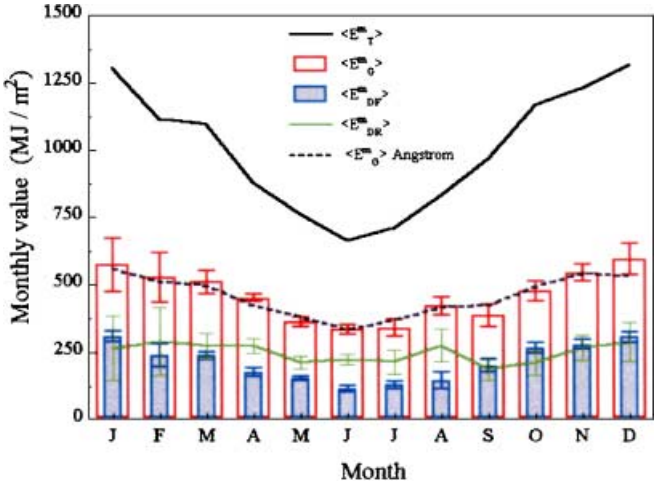

Fig. 9. Annual evolution of monthly values of solar radiation observed at IAG. The black dashed line represents the global solar radiation estimated using Angstrom formula. The error bars correspond to 95% confidence interval

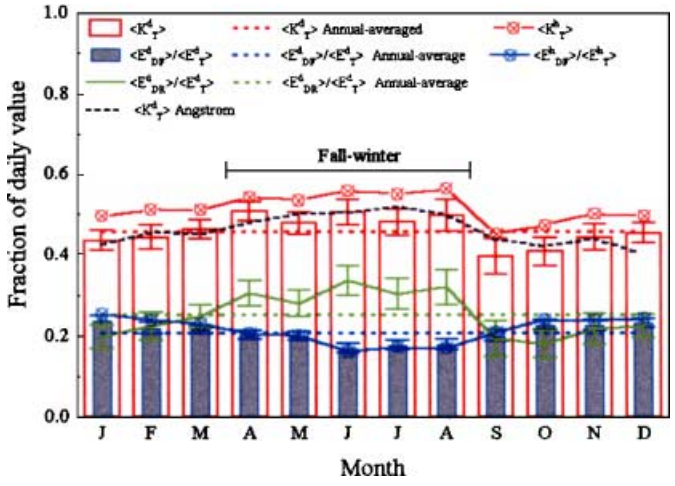

Fig. 10. Annual evolution of $\langle K_T^d \rangle$, $\langle E_{DF}^d \rangle / \langle E_T^d \rangle$ and $\langle E_{DR}^d \rangle / \langle E_T^d \rangle$ at IAG. The error bars correspond to 95% confidence interval. Values of $\langle K_T^h \rangle$ and $\langle E_{DF}^h \rangle / \langle E_T^h \rangle$ correspond to hourly values at 12:30 LT. The black dashed line represents the clearness index estimated using Angstrom formula. The annual-averaged values of $\langle K_T^d \rangle$, $\langle E_{DF}^d \rangle / \langle E_T^d \rangle$ and $\langle E_{DR}^d \rangle / \langle E_T^d \rangle$ are also displayed

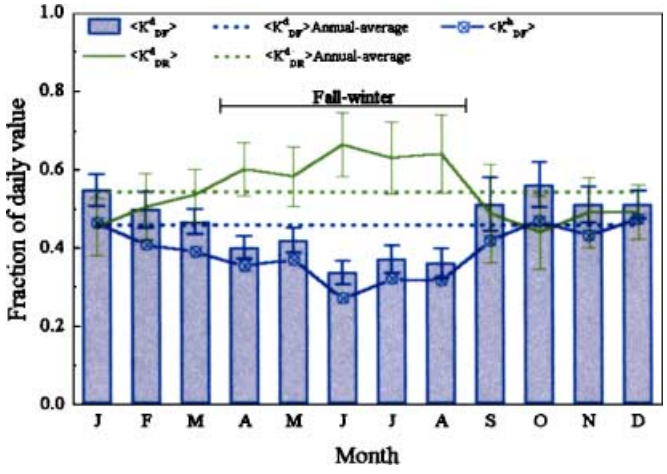

Fig. 11. Annual evolution of daily diffuse and direct fractions at IAG. The annual evolution of hourly diffuse fraction and of annual-average of $\langle K_{DF}^d \rangle$ and $\langle K_{DR}^d \rangle$ are also displayed. The error bars correspond to 95% confidence interval. The values $\langle K_{DF}^h \rangle$ correspond to observation at 12:30 LT

respectively, 27.1% and 57% smaller than in December, while the amplitude of $\langle E_{DR}^h \rangle$ is 1.6% larger (Table 1). This indicates that the atmosphere, at the peak hour, attenuates in June 43.7% less solar energy than in December.

Considering only daily values, it is observed that in June $\langle E_G^d \rangle$, $\langle E_{DF}^d \rangle$ and $\langle E_{DR}^d \rangle$ are, respectively, 42%, 61.7% and 21.7% smaller than in December (Table 1). This indicates that the atmosphere, on a daily basis, attenuates in June 52.9% less solar energy than in December.

June and December define the climate extremes in the City of São Paulo, which is characterized by a dry and cloudless winter and wet and cloudy summer. It is also observed that August is the driest month of the year (Fig. 2, top) and this dryness is reflected as a maximum value of global and direct components of the solar radiation in São Paulo (Figs. 7, 8 and 9).

The observed difference between the amplitude of the diurnal cycle and of the daily values can be due to the fact that the latter incorporates, implicitly, the duration of the day (which in June is 20.9% smaller than in December). Therefore, to use the amplitude of the diurnal evolution of the hourly values to characterize the climate of São Paulo City it is necessary to associate this information with the local duration of the day. In general, the magnitude of daily values is larger than the amplitude of the diurnal evolution of the hourly values.

The seasonal variability of the solar radiation in the City of São Paulo, can be summarized as: (a) in December there is twice as much solar

energy than in June; (b) in December the amount of energy associated with the diffuse component of solar radiation is three times larger than in June and (c) in December the amount of energy associated with the direct component of solar radiation is only four-third larger than in June.

4.2 Seasonal variability of the daily values of clearness index and radiation fractions

The seasonal variation of the daily values of the clearness index and diffuse and direct radiation fractions in the City of São Paulo (Figs. 10 and 11) indicates that $\langle K_T^d \rangle$ and $\langle E_{DR}^d \rangle / \langle E_T^d \rangle$ show larger values in winter and smaller values in summer months (Fig. 10). In the case of $\langle E_{DF}^d \rangle / \langle E_T^d \rangle$, the largest values occur in summer (Fig. 10). The annual evolution of $\langle K_T^d \rangle$ is systematically smaller than the annual evolution of the amplitude of $\langle K_T^h \rangle$, while the annual evolution of $\langle E_{DF}^d \rangle / \langle E_T^d \rangle$ coincides with the annual evolution of the amplitude of $\langle E_{DF}^h \rangle / \langle E_T^h \rangle$ (Fig. 10). This coincidence occurs because $\langle E_{DF}^h \rangle / \langle E_T^h \rangle$ is approximately constant during the daytime (Fig. 5).

The annual evolution of $\langle K_{DF}^d \rangle$, shown in Fig. 11, is proportional to the annual evolution of $\langle E_{DF}^d \rangle / \langle E_T^d \rangle$ (Fig. 10) while $\langle K_{DR}^d \rangle$ (Fig. 11) follows the annual evolution $\langle K_T^d \rangle$ (Fig. 11). This pattern is also present in the annual evolution of the amplitude of $\langle K_{DF}^h \rangle$ and $\langle K_{DR}^h \rangle$ (Fig. 6). The amplitude of $\langle K_{DF}^h \rangle$ (Fig. 6) is systematically smaller $\langle K_{DF}^d \rangle$ (Fig. 11).

When the annual-averaged values of these fractions are taken as reference (horizontal lines in Figs. 10 and 11), it is possible to classify the climate in the City of São Paulo into two distinct periods: (a) autumn–winter period, from April to August and (b) spring–summer period, from September to March. In the autumn–winter period, values of $\langle K_T^d \rangle$, $\langle K_{DR}^d \rangle$ and $\langle E_{DR}^d \rangle / \langle E_T^d \rangle$ are systematically larger than their annual-averaged values, while $\langle K_{DF}^d \rangle$ and $\langle E_{DF}^d \rangle / \langle E_T^d \rangle$ are systematically smaller. In the spring–summer period the opposite occurs.

This seasonal pattern can be explained in terms of the seasonal variation of the cloud cover and content of water vapor in the region of São Paulo. The largest values of $\langle E_{DR}^d \rangle / \langle E_T^d \rangle$ occur in the autumn–winter period, when cloud activity and moisture content are smaller (Fig. 2). The similarity between the annual evolution of monthly-averaged sunshine hours and cloudiness (Fig. 2, bottom) and the annual evolution of the fractions of monthly-values of solar radiation (Figs. 10 and 11) are remarkable. This indicates that the seasonal variation of hourly, daily and monthly values of solar radiation, presented here, capture the essence of climate conditions of the City of São Paulo.

4.3 Regional and local estimates of daily global and diffuse energy fluxes

To verify the representation of the data obtained at the IAG site for the region of São Paulo, the local characterization of solar radiation is compared with more regional estimates of daily values of global and diffuse solar radiation. Pereira et al. (1996) presented the only regional information available in the literature for São Paulo. They used satellite techniques and 2 years of solar radiation observations, from 22 surface stations distributed in Brazil, including one in the urban area of São Paulo, to build spatial maps of daily values of global and diffuse solar radiation.

The values of daily global and diffuse solar radiations, obtained from their map, are referred to here as regional values for São Paulo. The values measured at the IAG site are referred to as local values for São Paulo.

The regional values of $\langle E_G^d \rangle$ and $\langle E_{DF}^d \rangle$ for São Paulo during the winter months (June–August) are $14\,MJ/m^2$ and $5\,MJ/m^2$, respectively and the local values are $11.85\,MJ/m^2$ and $4.21\,MJ/m^2$ respectively. During the summer months (December–February) the regional values of $\langle E_G^d \rangle$ and $\langle E_{DF}^d \rangle$ are $22\,MJ/m^2$ and $9\,MJ/m^2$, respectively and the local values are $18.41\,MJ/m^2$ and $9.52\,MJ/m^2$, respectively.

Therefore, the local values of global solar radiation are systematically smaller ($\sim$16%) than the regional values, in both periods. The regional values of diffuse solar radiation are smaller in winter ($\sim$16%) and slightly larger in summer ($\sim$6%) than the local values. Even when the error bars are considered the discrepancies are significant (small solid circles in Fig. 8).

Given that the local and regional estimates are sufficiently accurate, then the discrepancies found can be attributed to (a) lack of time resolution in the regional estimates because it was performed using only 2 years of observation

and/or (b) the existence of large spatial variability in the solar radiation field in São Paulo. Local effects associated with spatial variability in the air pollution, topographic cloud or fog, and variation in the urban albedo can act to reduce, at the IAG site, the global and diffuse solar radiation during both periods. The following sections address these effects.

5. Variability of solar radiation during clear sky days

The annual evolution of the solar radiation in the City of São Paulo is related basically to the availability of moisture, as indicated in sections 3 and 4. For instance the driest period (autumn–winter) is associated with the smallest values of cloudiness (6 tenths, Fig. 2). Therefore, during this period, a larger concentration of days with clear sky would be expected.

Visual inspection of the diurnal evolution of 5 min-averaged irradiance values indicated the existence of 190 days with no clouds at the IAG site (Fig. 12). This corresponds to 10% of the whole period of observation (section 2) and, as expected, most of the clear sky days occurred during the autumn–winter period (Fig. 12, top). It is important to mention here that this result is not biased by an uneven distribution of number of days per month, as can be seen by Fig. 12 (bottom).

The distribution of the number of the days in classes of fractions of daily values of solar radiation (K_T^d, E_{DF}^d/E_T^d, E_{DR}^d/E_T^d, K_{DF}^d and K_{DR}^d) are very close to a Gaussian shape (Fig. 13). In the absence of clouds, 65.4% of solar energy incident

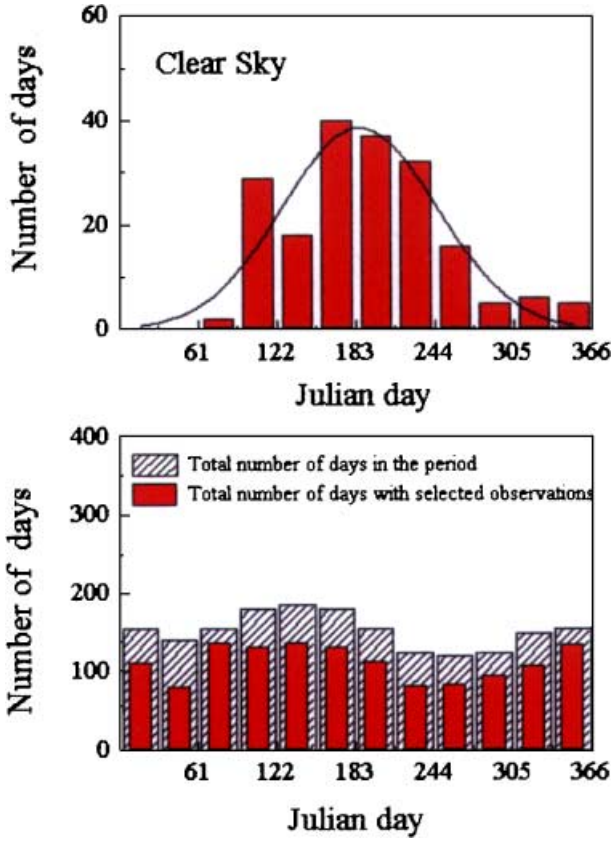

Fig. 12. Monthly distributions of total number of days with clear sky conditions (top) and number of days with simultaneous observation of global and diffuse solar radiation at IAG (bottom). Continuous line (top) corresponds to a Gaussian curve fitted through the histogram. Hatched areas (bottom) correspond to the total number of days in the period of observation

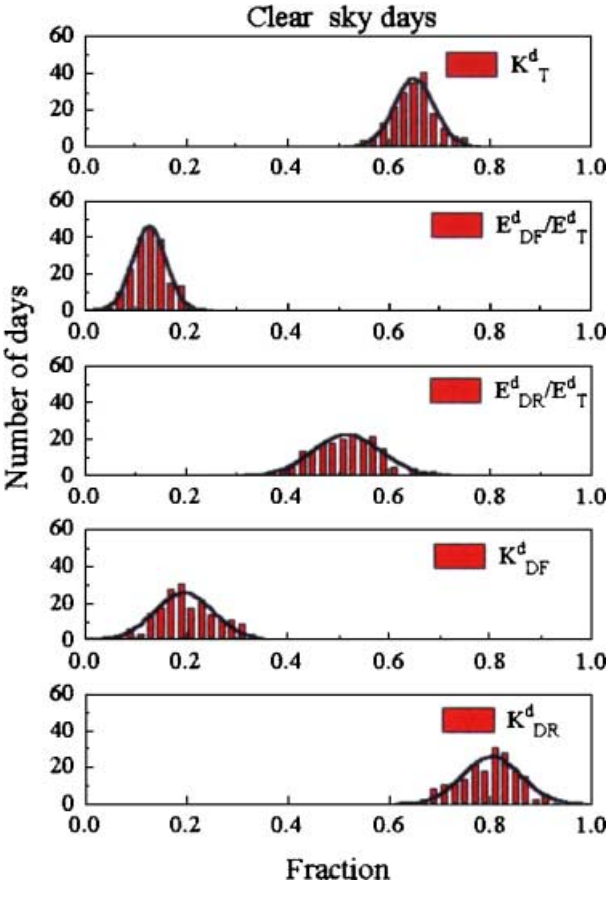

Fig. 13. Histogram of frequency of days by classes of K_T^d, E_{DF}^d/E_T^d, E_{DR}^d/E_T^d, K_{DF}^d and K_{DR}^d for days with clear-sky conditions in the IAG. Continuous lines correspond to Gaussian curves fitted through each histogram (see Table 1)

at the top of the atmosphere reaches the surface as global, 13.7% as diffuse and 51.7% as direct component (Table 1). Therefore, the behavior found during autumn–winter period, April–August, (Figs. 7–11) is controlled by the larger frequency of clear sky days during this period.

6. The air pollution effect on solar radiation at surface

To quantify the role played by air pollution upon solar radiation, an analysis was carried out that considered hourly particulate matter concentration values (diameter $\leq 10\,\mu m$) measured at a site (''Lapa'') located in the City of São Paulo, about 4 km away from the IAG site (Fig. 1). The particulate matter measurements were performed by CETESB (CETESB, 1999).

Here, the analysis was restricted to those days when particulate matter measured in the Lapa site correlated well with a second site, ''Cerqueira Cesar'', (Fig. 1). This procedure assures that values of particulate matter used here are representative of a wider area to include the IAG site. To avoid problems with clouds only days with clear sky conditions were considered, as described in section 5.

In summary, two criteria were utilized to choose the data to be analyzed. First, the presence of clear sky conditions and second the particulate matter observed at the Lapa site had to correlate well with the particulate matter observed at the Cerqueira Cesar site. Therefore, from the 190 days initially identified as clear sky conditions (section 5) 164 days were chosen.

The dispersion diagrams between the concentration of particulate matter and K_T indicates reductions of 10–12% in hourly and daily values (Fig. 14). These values were obtained by applying the fitted regression line over the observed range of concentrations of particulate matter. It may explain part of the discrepancies between local and the regional estimates of daily global solar radiation in São Paulo (section 4.3).

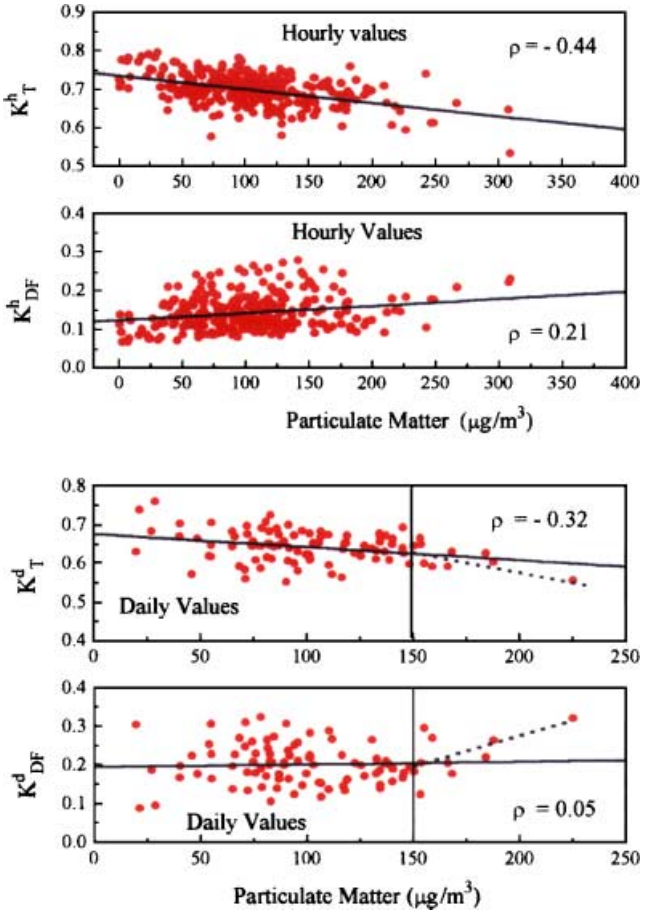

Fig. 14. Scatter diagram for K_T^h and K_{DF}^h versus hourly values of concentration of particulate matter and for K_T^d and K_{DF}^d versus daily-averaged values of concentration of particulate matter observed during clear-sky days. Hourly values correspond the period between 10:00 and 14:00 LT. The fractions were observed at IAG and the particulate matter was observed in Lapa site by CETESB. Continuous line corresponds to the fitted curve by linear regression and ρ is the coefficient of linear regression. The dashed lines represent the variations of K_T^d and K_{DF}^d when the concentration of particulate matter is greater than $150\,\mu g/m^3$

Although these results agree with the previous investigation carried out in the City of São Paulo (Oliveira et al., 1996) they must be considered with reservations. The linear correlation coefficients found between K_T^h and the hourly mean concentration of particulate matter ($\rho = -0.44$), and between K_T^d and the daily mean concentration of particulate matter ($\rho = -0.32$) – even though they are larger than the linear coefficient considering K_{DF}^h and K_{DF}^d ($\rho = 0.21$ and $\rho = 0.05$, respectively) – are still small ($|\rho| < 0.5$). If only the cases when the concentration of particulate matter are greater than $150\,\mu g/m^3$, (standard for 24 hours, according to Seinfeld, 1985) are considered, the variations of K_T^d and K_{DF}^d with the concentration of particulate matter appear to be more intense (dashed lines in Fig. 14).

7. Modeling the diurnal evolution of hourly values of global and diffuse solar radiation

Liu and Jordan (1960) were the first to estimate the diurnal evolution of the diffuse component in terms of daily values of the global solar radiation. A more modern approach to this question can be found in Aguiar and Collares-Pereira (1992).

The diurnal evolution of the monthly-averaged values of solar radiation – described in the sections 3 and 4 – indicate that the combined effect of the cloud and moisture makes the atmosphere in the City of São Paulo behave like a cloudless atmosphere with small broadband transmissivity (Gueymard, 1989). This characteristic allows the development of simple models to estimate the diurnal evolution of the monthly-averaged global and diffuse solar radiations, at the surface, in terms of the monthly-averaged hourly values of the solar radiation at the top of the atmosphere.

Here, a simple model is derived based on the observational fact that $\langle K_T^h \rangle$ and $\langle E_{DF}^h \rangle / \langle E_T^h \rangle$ have a very well defined diurnal evolution during all months of the year in São Paulo. Therefore, an expression for $\langle E_G^h \rangle$ and $\langle E_{DF}^h \rangle$ as a function of $\langle E_T^h \rangle$ can be obtained adjusting empirical functions to the observed diurnal evolution of $\langle K_T^h \rangle$ and $\langle E_{DF}^h \rangle / \langle E_T^h \rangle$.

For $\langle K_T^h \rangle$ the best adjustment (dotted line in the Fig. 5) was obtained by the following function:

$$\langle K_T^h \rangle = \frac{\langle E_G^h \rangle}{\langle E_T^h \rangle} = a_G + b_G \sin[\pi(t - t_0)/T] \qquad (2)$$

where a_G and b_G are constants, t is the time (local time), t_0 and T are, respectively, initial time (considered constant and equal to 06:00 LT) and period of the diurnal evolution of $\langle K_T^h \rangle$. The parameter values are indicated in Table 2. The linear correlation coefficient (ρ_G), associated with the linear regression fitting, varies from 0.951 (February) to 0.998 (July), indicating a very good match for all months of the year.

For $\langle E_{DF}^h \rangle / \langle E_T^h \rangle$ the best choice (solid lines in Fig. 5) is:

$$\langle E_{DF}^h \rangle / \langle E_T^h \rangle = a_{DF} \qquad (3)$$

where a_{DF} is a constant estimated as the daytime-averaged of $\langle E_{DF}^h \rangle / \langle E_T^h \rangle$ and shown in Table 2.

When compared with observations, model results reproduce very well the monthly-averaged daily values of global and diffuse solar radiation in the City of São Paulo for all months of the year (Table 2). Taking the observed value of $\langle E_G^d \rangle$ as reference, it can be verified that $\int_{t_1}^{t_2} \langle E_G^h \rangle dt$ (with $\langle E_G^h \rangle$ given by expression (2)) lies between -0.6% (in May) and $+0.1\%$ (in September). The values $\int_{t_1}^{t_2} \langle E_{DF}^h \rangle dt$ (with $\langle E_{DF}^h \rangle$ given by expression (3)) are located within -6.0% (June) and $+4.4\%$ (December) of $\langle E_{DF}^d \rangle$. The annual evolution of period T (Table 2) in expression (2) is directly related to the annual distribution of monthly sunshine hours (Fig. 2, bottom). This explains the good performance of these expressions (and the Angstrom expression described in section 8 below) for daily values of global solar radiation in the City of São Paulo.

The diurnal evolution of $\langle K_{DF}^h \rangle$, estimated from expressions (2) and (3) considering $\langle K_{DF}^h \rangle = (\langle E_{DF}^h \rangle / \langle E_T^h \rangle) / \langle K_T^h \rangle$, are indicated in Fig. 6 (dotted lines). According to Fig. 6, the match is not as good as the one obtained for $\langle K_T^h \rangle$ and $\langle E_{DF}^h \rangle / \langle E_T^h \rangle$. However, most of the modeled values are located within the statistical error bar range.

Finally, the fact that all the modeled values of $\langle E_G^h \rangle$ and $\langle E_{DF}^h \rangle$ (dotted lines in Figs. 4 and 7) are located within the interval of 95% confidence (error bars), indicates that these models reproduce satisfactorily the diurnal evolution of these

Table 2. Annual variation of parameters used to estimate diurnal evolution of monthly averaged values of global and diffuse solar radiation at surface in São Paulo. Parameter ρ_G is the correlation coefficient for $\langle K_T^h \rangle$, t_1 and t_2 correspond to local time of sunrise and sunset. The variables t corresponds to local time in hours and t_0 is equal 6:00 LT. T is the period of observed diurnal evolution. The errors were estimated considering (modeled value − observed value)/(observed value)

Month	$\langle K_T^h \rangle = a_G + b_G \sin[\pi(t - t_0)/T]$						$\langle E_{DF}^h \rangle / \langle E_T^h \rangle = a_{DF}$			
	a_G	b_G	T	ρ_G	$\int_{t_1}^{t_2} \langle E_G^h \rangle dt$	$\langle E_G^d \rangle$ (Obs.)	Error (%)	a_{DF}	$\int_{t_1}^{t_2} \langle E_{DF}^h \rangle dt$	$\langle E_{DF}^d \rangle$ (Obs.)	Error (%)
Jan.	0.23	0.27	12.50	0.973	18.31	18.30	0.1	0.23	9.68	10.00	−3.2
Feb.	0.19	0.34	12.00	0.951	17.62	17.64	−0.1	0.21	8.44	8.75	−3.5
Mar.	0.17	0.36	13.00	0.968	16.35	16.36	−0.1	0.21	7.29	7.63	−4.5
Apr.	0.21	0.35	14.00	0.977	14.96	14.99	−0.1	0.20	5.86	6.00	−2.3
May	0.12	0.43	13.75	0.994	11.69	11.76	−0.6	0.20	4.88	4.92	−0.8
Jun.	0.08	0.50	13.75	0.994	11.21	11.21	0.0	0.16	3.45	3.67	−6.0
Jul.	0.07	0.48	14.00	0.998	11.04	11.10	−0.5	0.18	4.03	4.04	−0.2
Aug.	0.11	0.46	14.00	0.992	13.29	13.34	−0.4	0.18	4.78	4.79	−0.2
Sep.	0.12	0.34	13.25	0.992	12.72	12.71	0.1	0.19	6.16	6.49	−5.1
Oct.	0.18	0.29	12.50	0.990	15.34	15.34	0.0	0.22	8.27	8.59	−3.7
Nov.	0.22	0.29	13.75	0.981	18.07	18.09	−0.1	0.22	8.86	9.23	−4.0
Dec.	0.28	0.23	12.00	0.968	19.20	19.26	−0.3	0.24	10.27	9.84	+4.4

parameters and their annual variation in São Paulo. Thus, despite the simplicity, the expressions (2) and (3) and parameters described in Table 2, can be used to estimate, in terms only of $\langle E_T^h \rangle$, the diurnal evolution of the monthly-averaged hourly values of global and diffuse solar radiation during all months of the year for the City of São Paulo. In summary, it is possible to estimate the monthly average of the direct component of the solar radiation knowing the diurnal evolution of hourly values of solar radiation at the top of atmosphere.

8. Modeling daily and monthly values

The Angstrom formula is the most popular, and also the most tested, method of estimating monthly-averaged daily values of global solar radiation at the surface, available in the literature. According to Newland (1989) best results can be obtained from the following version of Angstrom formula:

$$\langle K_T^d \rangle = 0.18 + 0.615 \langle S \rangle / \langle S_m \rangle \qquad (4)$$

where $\langle S \rangle$ and $\langle S_m \rangle$ are monthly-averaged daily sunshine hours and maximum daily sunshine hours. This expression is valid for 40°S–40°N and can therefore be applied to estimate the global solar radiation in São Paulo.

Considering the annual evolution of $\langle S \rangle$, for the City of São Paulo, obtained from observations carried out between 1961 and 1990 (Fig. 2) at Mirante de Santana (Fig. 1), expression (4) was applied to estimate $\langle K_T^d \rangle$ and, using the calculated values of $\langle E_T^d \rangle$ it was estimated $\langle E_G^d \rangle$. The values of $\langle E_G^d \rangle$, $\langle E_G^m \rangle$ and $\langle K_T^d \rangle$ estimated from expression (4), are indicated in Figs. 8, 9 and 10, respectively (black dashed-lines labeled by Angstrom). Except for December, the modeled values are within the range given by the error bars, indicating a very good match between observed and modelled values.

For $\langle E_G^d \rangle$, this agreement corroborates with the fact that the global solar radiation measurements carried out at the IAG site are representative of the climate conditions in the City of São Paulo. This also indicates that the discrepancies between the local measurements and the more regional estimates obtained from satellite data (Pereira et al., 1996) are not related to observational problems.

9. Conclusion

Measurements of global solar radiation at the surface and its diffuse component carried out in the City of São Paulo between 1994 (April 26) and 1999 (June 30) are used to characterize the seasonal evolution of hourly, daily and monthly values of global, diffuse and direct solar radiation, the clearness index, and diffuse and direct fractions.

Aging effects induced by continuous exposure of the sensors to the urban environment and blocking effects caused by the shadow-band were taken into consideration explicitly leading to the following results:

- Comparatively, the use of estimated calibration constants make the global solar radiation values 3.5% smaller and the diffuse component 4.4% larger. The related fractions are influenced by the combined effect of these variations inducing variations from 3.5% (clearness index) to 7.9% (direct and diffuse fractions). The impact caused by these variations is small and located within the intervals of variation of the hourly, daily and monthly values for a 95% confidence level during all months of the year;
- The Diffuse solar radiation measured by shadow-band and corrected for blocking effects are about 10% smaller than the pyrheliometer estimates. This discrepancy is due to the fact that the expression used to correct the blocking effect (Eq. 1), does not take into consideration the anisotropy of the diffuse solar radiation field. This effect is particularly important in the City of São Paulo due to the large concentration of particulate matter in the local atmosphere. However, more investigation will be necessary to take this effect into consideration in the estimates of diffuse solar radiation in São Paulo;
- Monthly-averaged hourly values of global solar radiation, diffuse and direct components, the clearness index, and diffuse and direct fractions have a statistically significant diurnal cycle (with 95% of confidence);
- The amplitude of the diurnal cycle of these quantities can be expressed in terms of their monthly-averaged hourly values at 12:30 LT;
- The seasonal evolution of the diurnal cycle can be used to typify the local climate when associated with monthly-averaged values of sunshine period, that in turn is equivalent to the daily or monthly values;
- The annual evolution of monthly-averaged hourly values of solar radiation at the surface indicates the existence of a seasonal pattern with two periods: (a) autumn–winter period, from April to August; and (b) spring–summer period, from September to March;
- In the autumn–winter period, daily and monthly values of global solar radiation – at the top of the atmosphere and at the surface – are half of the values available in the spring–summer period;
- In the autumn–winter period, the daily and monthly values of diffuse (also hourly) and direct components are, respectively, about one-third and three-quarters of the solar energy available in the spring–summer period;
- About 10% of the days in the City of São Paulo are characterized by clear sky conditions, and most of them are observed in the period between April and August (autumn–winter period);
- Observed monthly-averaged daily values of global and diffuse solar radiation at the IAG site are lower than the regional values proposed by Pereira et al. (1996) during winter and summer months;
- Air pollution events, such as the high concentration values of the particulate matter, may cause significant reductions (10–12%) in the hourly (and daily) values of global solar radiation at the surface. The expected increase in monthly-averaged hourly and daily values of the diffuse component of the solar radiation at the surface were not observed, indicating that absorption of solar radiation by the polluted urban atmosphere may have an important effect in São Paulo. The lack of information about the radiative characteristics of the aerosol in São Paulo precluded any further conclusion, and need to be investigated. The discrepancy between the regional estimates (Pereira et al., 1996) and our estimates can be explained in terms of the air pollution effects, which seem to reduce the global values of the solar radiation at the surface in São Paulo. Surprisingly, this reduction was not followed by an expected increase in the diffuse component of the solar radiation, at the surface, as observed in the previous work by Oliveira et al. (1996). These results confirm that any extrapolation from the

observations of solar radiation carried out in the urban regions should be made carefully (Longuetto et al., 1992);

- Monthly-averaged hourly values of global and diffuse solar radiation are successfully estimated by the following expressions: $\langle K_T^h \rangle = a_G + b_G \sin[\pi(t - t_0)/T]$ and $\langle E_{DF}^h \rangle / \langle E_T^h \rangle = a_{DF}$ for all months of the year (Table 2);
- Monthly-averaged daily values of global solar radiation at the surface are satisfactorily simulated by the Angstrom's expression, proposed by Newland (1989), $\langle K_T^d \rangle = 0.18 + 0.615 \langle S \rangle / \langle S_m \rangle$, where $\langle S \rangle$ and $\langle S_m \rangle$ are monthly-averaged daily sunshine hours and monthly-averaged daily maximum sunshine hours, respectively;

Finally, the amount of solar energy per unit area reaching the surface as direct beam is $3.0\,GJ/m^2$ per year. This value corresponds to a total of 6,633 TWh per year in the whole area of MRSP. This amount of energy is equivalent to 0.6% of energy consumption (40 TWh) in this region during one year (Eletropaulo, 1999). Taking into consideration the environmental problems associated with all other sources of energy, it seems reasonable to consider solar energy as a valid alternative energy source in the Metropolitan Region of São Paulo.

Acknowledgements

The authors acknowledge the financial support provided by the ''Conselho Nacional de Desenvolvimento Científico e Tecnológico'' and ''Fundação de Amparo à Pesquisa do Estado de São Paulo''.

References

Aguiar R, Collares-Pereira M (1992) Statistical properties of hourly global radiation. Solar Energy 48: 157–167

Burek SAM, Norton B, Probert SD (1988) Analytical and experimental methods for shadow-band correction factors for solarimeters on inclined planes under isotropically diffuse and overcast skies. Solar Energy 40: 151–160

CETESB (1999) Technical Report (in Portuguese)

Collares-Pereira M, Rabl A (1979) The average distribution of solar radiation – correlation between diffuse and hemispherical and between daily and hourly insolation values. Solar Energy 22: 155–164

Duffie JH, Beckman WH (1980) Solar engineering of thermal processes. New York: Wiley Interscience

Eletropaulo (1999) Technical Report (in Portuguese)

Erbs DG, Klein SA, Duffie JA (1982) Estimation of the diffuse radiation fraction for hourly, daily and monthly-average global radiation. Solar Energy 28: 293–302

Escobedo JF, Frisina VA, Chaves MA, Oliveira AP (1997) Radiômetros solares com termopilhas de filmes Finos II Desempenho Revista Brasileira de Aplicações de Vácuo 16: 16–21 (in Portuguese)

Frölich C, Lean J (1998) The sun's total irradiance: Cycles and trends in the past two decades and associated climate change uncertainties. Geophys Res Lett 25: 4377–4380

Garrison J, Sahami K (1995) A study of the division of global irradiance into direct beam and diffuse irradiance at seven Canadian sites. Solar Energy 55: 493–504

Gueymard C (1989) A two-band model for the calculation of clear sky solar irradiance, illuminance, and photosynthetically active radiation at the earth's surface. Solar Energy 44: 253–265

Ineichen P, Gremand JM, Guisau O, Mermond A (1984) Study of the corrective factor involved when measuring the diffuse solar radiation by us of the ring method. Solar Energy 32: 585–590

Iqbal M (1983) An introduction to solar radiation. New york: Academic Press, 390 pp

Iziomon MG, Aro TO (1999) On the annual and monthly mean diurnal variation of diffuse solar radiation at a meteorological station in West Africa. Meteorol Atmos Phys 69: 223–230

Jacovides CP, Hadjioannou L, Passhiardis S, Stefanou L (1996) On the diffuse fraction of daily and monthly global radiation for the Island of Cyprus. Solar Energy 56: 565–572

Kretzschmar JG (1994) Particulate matter levels and trends in Mexico City, São Paulo, Buenos Aires and Rio de Janeiro. Atmos Environ 28: 3181–3191

LeBaron BA, Peterson WA, Girmhirn I (1980) Corrections for diffuse Irradiance measured with shadowbands. Solar Energy 25: 1–13

LeBaron BA, Dirmhirn I (1983) Strengths and limitations of the Liu and Jordan model to determine diffuse from global irradiance. Solar Energy 31: 167–172

LeBaron BA, Michalsky JJ, Perez R (1990) A simple procedure for correcting shadowband data for all sky conditions. Solar Energy 44: 249–256

Liu BYH, Jordan RC (1960) The interrelationship and characteristic distribution of direct, diffuse and total solar radiation. Solar Energy 4: 1–9

Longuetto A, Giacomelli L, Giraud G, Zaramella G (1992) A study of correlation among solar energy, atmospheric turbidity and pollutants in urban area. Atmos Environ 26B: 29–43

INMET (2000) Instituto Nacional de Meteorologia do Brasil (http://www.inmet.br).

Mello JMD (1993) Desenvolvimento de um sistema para medir simultaneamente radiações global, difusa e direta. Tese de Doutorado, Faculdade de Ciências Agronômicas, Unesp-Botucatu, SP, Brazil, 130 pp (in Portuguese)

Newland FJ (1989) A study of solar radiation modes for the coastal region of South China. Solar Energy 43: 227–235

Oke TR (1982) The energetic basis of urban heat island. Quart J Roy Meteor Soc 108: 1–24

Oliveira AP, Escobedo JF, Plana-Fattori A, Soares J, Santos PM (1996) Medidas de radiação solar na Cidade de São

Paulo: Calibração de piranômetros e aplicações meteorológicas. Revista Brasileira de Geofísica 14: 203–216 (in Portuguese)

Panitzer HH (1983) The shade ring correction for diffuse irradiance measurements. Solar Energy 26: 361–363

Pereira EB, Abreu SL, Stuhlmann R, Reiland M, Colle S (1996) Survey of the incident solar radiation in Brazil by use of Meteosat satellite data. Solar Energy 57(2): 125–132

Petterson JT, Flowers EC, Rudisill JH (1978) Urban-rural solar radiation and atmospheric turbidity measurements in the Los Angeles Basin. J Appl Meteor 17: 1595–1609

Rawlins F, Readings CJ (1986) The shade ring correction for measurements of diffuse irradiance under clear skies. Solar Energy 37: 407–416

Satyamurty VV, Lahiri PK (1992) Estimation of symmetric and asymmetric hourly global and diffuse radiation from daily values. Solar Energy 48: 7–14

Seinfled JH (1985) Atmospheric chemistry and physics of AIR POLLUTION. New york: Wiley-Interscience, 738 pp

Siren KE (1987) The shadow band correction for diffuse irradiation based on a two component sky radiation model. Solar Energy 39: 433–438

Soler A (1990) Dependence on latitude of the relation between the diffuse fraction of solar radiation and the ratio of global-to-extraterrestrial radiation for monthly average daily values. Solar Energy 44: 297–302

Stanhill G (1985) Observations of shade-ring correction factors for diffuse sky radiation measurements at the Dead Sea. Quart J Roy Meteor Soc 111: 1125–1130

Steven MD (1984) The anisotropy of diffuse sky radiation determined from shade-ring measurements. Quart J Roy Meteor Soc 110: 261–270

WMO (1971) Guide to meteorological instruments and observing practices. Fourth Edition, Geneva, Secretariat of the World Meteorological Organization, publication WMO N^{o} 8, 325 pp

Authors' addresses: Amauri P. de Oliveira (e-mail: apdolive@usp.br), Antonio J. Machado, Jacyra Soares, Group of Micrometeorology, Department of Atmospheric Sciences, Institute of Astronomy and Geophysics, University of São Paulo, Rua do Matão, 1226, 05508.900 – São Paulo, SP, Brazil; João F. Escobedo, Laboratory of Solar Radiation, Department of Environmental Sciences, State University of São Paulo – UNESP, Botucatu, SP, Brazil.